Fatigue behaviour of toe and root stiffener cracks in stiffener-to-deck plate weld of orthotropic bridge decks

Wu, Weijian; Veljkovic, Milan; Kolstein, Henk; Maljaars, Johan; Pijpers, Richard

DOI
10.1016/j.engstruct.2024.117740

Publication date
2024

Document Version
Final published version

Published in
Engineering Structures

Citation (APA)
Wu, W., Veljkovic, M., Kolstein, H., Maljaars, J., & Pijpers, R. (2024). Fatigue behaviour of toe and root stiffener cracks in stiffener-to-deck plate weld of orthotropic bridge decks. *Engineering Structures*, *305*, Article 117740. https://doi.org/10.1016/j.engstruct.2024.117740

Engineering Structures 305 (2024) 117740

Contents lists available at ScienceDirect

Engineering Structures

journal homepage: www.elsevier.com/locate/engstruct

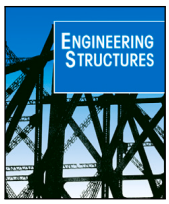

Fatigue behaviour of toe and root stiffener cracks in stiffener-to-deck plate weld of orthotropic bridge decks

Weijian Wu [a,*], Milan Veljkovic [a], Henk Kolstein [a], Johan Maljaars [b,c], Richard Pijpers [b]

[a] Delft University of Technology, Mekelweg 5, Delft, The Netherlands
[b] TNO, Molengraaffsingel 8, Delft, The Netherlands
[c] Eindhoven University of Technology, Blauwe Zaale 1, Eindhoven, The Netherlands

ARTICLE INFO

Keywords:
Orthotropic bridge deck
Toe and root stiffener cracks
Fatigue resistance
Structural stress
Local assessment methods

ABSTRACT

Fatigue cracks in the stiffener-to-deck plate connections of orthotropic bridge decks, initiating from the weld toe or root and propagating into the stiffener or weld throat, are experimentally and numerically studied. A statistical analysis of the structural stress is carried out using the experimental data. Automatic welded specimens show a significantly higher fatigue resistance than manual welded ones for both details of the study. Including results in the literature, the characteristic fatigue resistances appear larger than the values in current standards and range between 100 and 160 MPa. A proposal for the fatigue resistance values is given for design purposes. The effective notch stress, averaged strain energy density factor, and fracture mechanics methods are employed to study the sensitivity of the weld toe and root cracks for different (geometrical) variations, such as the lack of weld penetration. Among them, the fracture mechanics method agrees best with the experimental data. With the increase of weld penetration ratios from 75% to 100%, the fracture mechanics predicted fatigue resistances remain approximately equal for the weld toe cracks and increase for the weld root cracks.

1. Introduction

Steel Orthotropic Bridge Decks (OBDs) have been widely used in steel bridges, especially in long-span and in movable bridges since the first application in the years 1940. The advantages of low self-weight and large load-carrying capacity (resistance) make them attractive. An OBD consists of a deck plate supported by longitudinal (traffic flow direction) stiffeners (open or closed shapes) and transverse cross-beams. Direct loaded by wheels of heavy vehicles, OBDs experience millions of loading cycles in their service life. A large number of welded connections (joints) cause significant stress concentrations, and the combination makes OBDs sensitive to fatigue cracking, mainly initiating from one of the welded connections. Their fatigue performance now dominates the design and life cycle performance. Fatigue cracks were reported in the stiffener-to-deck plate, crossbeam-to-deck plate, deck plate-to-deck plate, crossbeam-to-stiffener, stiffener-to-stiffener welds (and some in the base material) [1,2]. Fatigue cracks may initiate from the weld toe or root, and propagate into base material or weld material. Stiffener-to-deck plate weld is of special interest because a large fraction of fatigue cracks were detected in practice [3,4]. Fig. 1 shows four types of cracks observed in this connection between the crossbeams, named according to [5]. Fatigue cracks of details C1a, C1b, and C2a propagate into base material. The fatigue crack of detail C2b propagate into weld material. The weld root cracks usually have a lower fatigue resistance as compared to cracks initiating from the weld toe because of the high notch effect, the lack of control of the weld root quality, and the higher crack propagation rate in weld material compared to base material [6]. However, the local stress ranges relevant to the four types of cracks in Fig. 1 are not (or not necessarily) equal. The geometry of weld, with the penetration ratio, is identified as an important parameter affecting the appearance of cracks [7]. A smooth weld profile and sufficient penetration ratios (minimum 75% to 80% of stiffener thickness but not melt-through) appear beneficial for fatigue resistance.

S-N curves are commonly used for design verification of high-cycle fatigue of OBDs. The Basquin relationship is applied for the number of cycles to failure N_R as a function of the applied stress ranges $\Delta\sigma$, see Eq. (1). The parameters m and a_N depend on the details and failure types. The characteristic value, $\Delta\sigma_C$ used in the European standard (pr)EN1993-1-9 [9,10], is linked to a_N and it is defined as the stress range associated with the number of cycles that has a 95% exceedance level of $N_R = 2 \times 10^6$ assuming a fixed slope parameter of $m = 3$. The values of a_N and $\Delta\sigma_C$ are obtained by a statistical analysis of the

* Corresponding author.
E-mail address: w.wu-1@tudelft.nl (W. Wu).

https://doi.org/10.1016/j.engstruct.2024.117740
Received 26 June 2023; Received in revised form 15 January 2024; Accepted 20 February 2024
Available online 6 March 2024

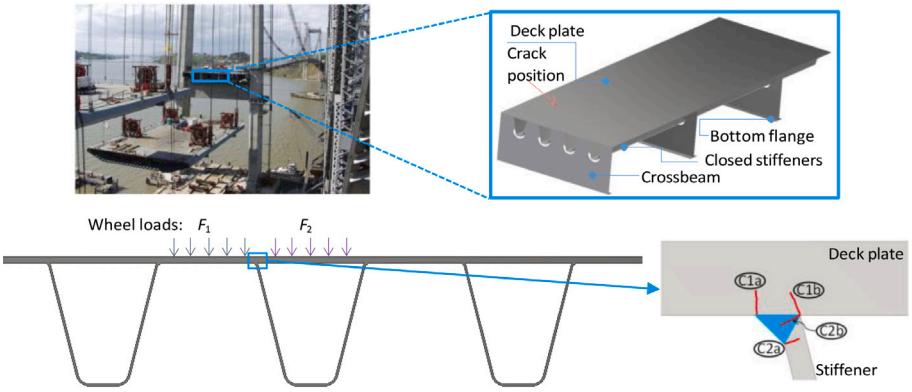

Fig. 1. Sketch of a representative OBD and stiffener-to-deck plate cracks in details.
Source: Construction site photo [8].

Table 1
$\Delta\sigma_C$ of welded steel plate connections in bridge guidelines.

Source	Method	Application	m_1	$\Delta\sigma_C$ [MPa]
[9–12]	NS	T & R	3 or 5	36 to 125
[9–12]	HSS	T	3	80 [11] or 90 or 100
[10]	ENS	T & R	3	200 or 225

experimental results.

$$log N_R = a_N - m \cdot log \Delta\sigma \quad (1)$$

In fatigue design, the Nominal Stress (NS) method is commonly used in the European guideline (pr)EN1993-1-9 [9,10], Japanese guideline [11], and AASHTO specifications [12]. The NS is computed without considering stress concentrations. Alternatively, the well-known (structural) Hot Spot Stress (HSS) method can be adopted for weld toe cracks [5,9,10,12], which considers the geometric stress concentrations in the stress computation and is accompanied by different fatigue resistances. The Effective Notch Stress (ENS) method analyses the local stress of the fictitious notch at crack initiation positions, which can be used for either weld toe or weld root cracks [9,10]. Table 1 summarizes $\Delta\sigma_C$ recommended in the commonly used bridge guidelines. However, because of load shedding, size effects and loading mode effects (the degree of bending and/or the fraction of compression stress), the fatigue resistance appears to depend on the detail type of OBDs, even when using structural or local stress parameters [2]. The values for $\Delta\sigma_C$ of the HSS and ENS methods in [9–12] therefore appear not always suited for the details in OBDs.

The averaged Strain Energy Density (SED) factor method is an energy-based approach using the averaged SED over a finite volume to predict the fatigue resistance of metal with sharp notches [13,14]. The Notch Stress Intensity Factors (NSIFs), a fatigue crack initiation parameter, can be calculated using SED, which depends on the opening angle of the notch. Analytical equations are proposed for notches with specific opening angles of 0° or 135° [15,16]. In more general applications, SED as an energy value can be directly obtained from Finite Element (FE) calculations. This method provides the possibility to analyse the energy state of the crack initiation position at the "microstructural support length" level [15]. A fitting procedure was carried out in [15] using more than 750 fatigue data for welded steel and aluminium joints to obtain the characteristic fatigue resistance and the slope parameter, resulting in a characteristic fatigue resistance (at 97.7% survival probability) of 0.058 N mm/mm^3 associated with a radius $R_0 = 0.28$ mm for the volume over which the SED was averaged for structural steel. A fixed slope parameter, $m = 1.5$, was used in the Basquin relation for the energy parameter using a linear elastic material.

The propagation period dominates the total fatigue life of welded connections due to the presence of sharp notches and initial imperfections [17]. Fracture mechanics, therefore, can be used for the analysis of the crack propagation period by analysing the stress state at the crack tip. In the Linear Elastic Fracture Mechanics (LEFM) framework, crack propagation can be described and predicted by the Paris' equation [18] or variations thereof, which provides the relationship between the stress intensity factor range and the crack propagation rate.

In stiffener-to-deck plate weld, the structural stress method was employed for the evaluation of the deck plate using the surface extrapolation approach [19–21] or the force equilibrium approach [22,23]. The local stress state was evaluated by the ENS [20,24,25]. Fatigue resistance calculation was executed using the LEFM [7,26,27]. However, most of these studies considered cracks in the deck plate (types C1a and C1b). A systematical study of stiffener cracking (types C2a and C2b) in modern OBDs using one of the aforementioned methods (NS, HSS, ENS, SED or LEFM) is lacking. It is unknown if (one of) these methods is suited for these types of cracks.

The few former studies into details C2a and C2b found in the literature [24,28–30] were carried out with automatic welding. In actual applications, however, manual overhead welds are also applied to connect OBD pannels on site. A series of fatigue tests is, therefore, carried out in the Stevin 2 Marco lab of Delft University of Technology to study the fatigue behaviour of details C2a and C2b. Automatic welded specimens (Series 1) and manual welded specimens (Series 2) are tested to study the effect of the welding procedure on the fatigue resistance of the details. Plane strain FE models are built in which the ENS, SED, and LEFM methods are applied to evaluate the effect of different weld penetration levels as presented in Section 4. The weld crack propagation is analysed by the LEFM using the eXtended Finite Element Method (XFEM). A fatigue assessment is determined from the stress state results using the local methods and reference values for the associated fatigue resistances in [6,31,32]. Using the authors' experiments and results in the literature, the fatigue resistances of details C2a and C2b are quantified by statistical analysis using the surface extrapolation obtained and force equilibrium obtained structural stress, respectively. The results can be used in the fatigue design guidelines of OBDs, e.g., Technical Specification TS 1993-1-901 "Fatigue design of orthotropic bridge decks with the hot spot stress method" that will be part of the second generation of Eurocodes [5].

2. Experimental study

2.1. Specimens

Two large welded stiffener-to-deck plate specimens have been fabricated using the steel grade S355J2, with a nominal yield stress of 355 MPa [33]. Fig. 2 provides the dimensions of the large specimens. A

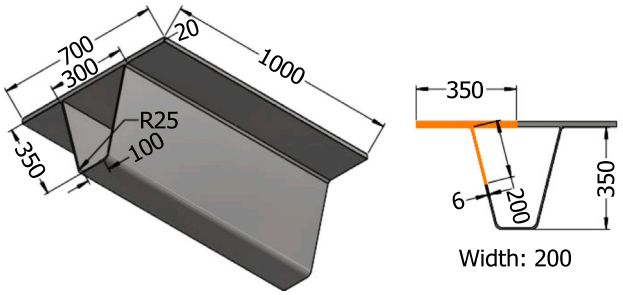

Fig. 2. Preparation of the specimens, left: uncut specimen, right in orange: test specimen, (unit: mm). (For interpretation of the references to colour in this figure legend, the reader is referred to the web version of this article.)

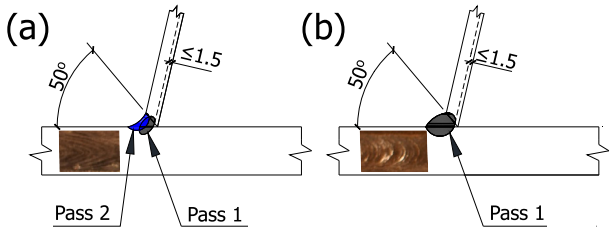

Fig. 3. Welding procedure of: (a) S1; (b) S2, and the representative weld surface photos (unit: mm).

6 mm thick trapezoid closed stiffener is welded to a $700\times1000\times20$ mm^3 deck plate each. In practice, the deck plate thickness varies significantly (between 10 to more than 20 mm) while the stiffener is more uniform (6 or 8 mm). Fatigue behaviour of OBDs with 10 to 12 mm thick plates, commonly seen in past, has been studied [1]. In modern OBDs, thicker deck plates are becoming popular due to the increase in traffic flow and fatigue problems with existing OBDs. Deck plates ranging from 16 mm to 19 mm can be seen in modern OBDs [8,34,35]. In the Netherlands, Schiphol bridge, Suurhoff bridge and the intended replacement of the Van Brienenoord bridge use the deck plate with a minimum thickness of 20 mm. The plate thickness affects the cooling rates and thereby the welding-induced residual stress. A 20 mm thick deck plate with 6 mm thick stiffener is selected to study the fatigue behaviour of stiffener cracks (types C2a and C2b). The effect of deck plate thickness can then be studied by comparing the results of the current study with those of [28,29]. Fig. 3 shows the details of the welding procedures. The stiffener edge is chamfered to an angle of 50°. The lack of weld penetration is specified to be 1.5 mm maximum (equal to 75% penetration ratio minimum) following [5,10]. Melt-through is not allowed. The actual penetration ratio is hence between 75% and 100%, but probably closer to the lower bound to reduce the risk of melt-through. The difference between the two is the welding procedure applied. Series 1 (S1) is automatically welded by two passes using Flux-Cored Arc Welding (FCAW) and Submerged Arc Welding (SAW), whereas Series 2 (S2) is manually welded by one pass using Shielded Metal Arc Welding (SMAW). Table 2 gives the applied welding parameters, with illustration in Fig. 4. S1 shows a smoother weld surface than S2. The welds of both series comply with the required quality level, namely, quality level B of ISO 5871 [36]. Nine and ten small specimens are cut, shown in orange in Fig. 2. Each specimen contains a deck plate with a size of $350\times200\times20$ mm^3 and a stiffener of $200\times200\times6$ mm^3.

2.2. Experimental programme

A load frame is built for the cyclic loading tests, as shown in Fig. 5. The deck plate is clamped onto an inclined steel plate by bolt heads so

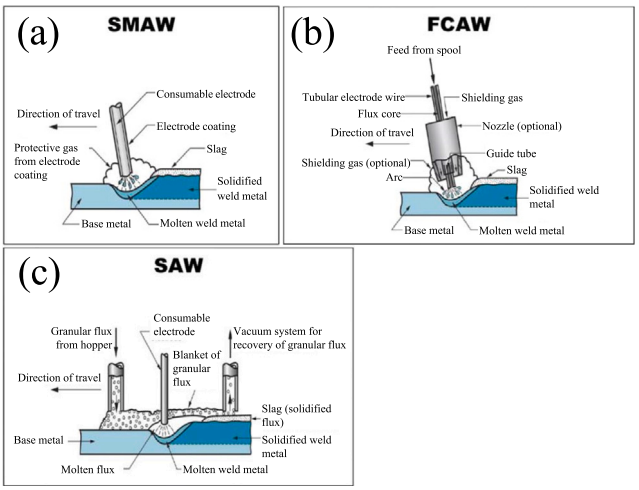

Fig. 4. Illustration of the applied welding procedures: (a) Shielded Metal Arc Welding (SMAW), (b) Flux-Cored Arc Welding (FCAW), and (c) Submerged Arc Welding (SAW) [37].

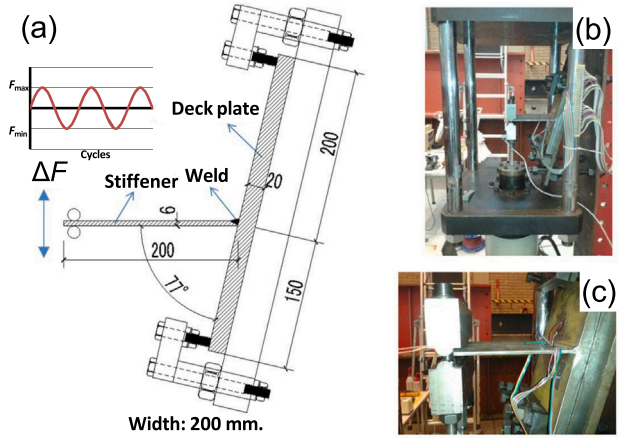

Fig. 5. Stiffener-to-deck welded connection and the setup for fatigue testing (unit: mm).

Table 2
Welding parameters used in the fabrication of the specimens.

Series	1	1	2
Pass	1	2	1
Process	FCAW	SAW	SMAW
Wire diameter [mm]	1.2	3	4
Current [A]	230–240	400–420	160–170
Voltage [V]	25–27	27–28	23–24
Current type	DC+	DC+	DC+
Welding speed [cm/min]	42–48	50–55	8–10
Heat input [kJ/mm]	0.7–1.0	1.2–1.4	2.3–2.8

that the stiffener is positioned horizontally. Two steel rollers are placed at the edge of the stiffener where the load is applied. Cyclic loading with a load ratio of $R = -1$ is applied through a hydraulic jack. The load ratio is relatively high compared to the actual stress condition in OBDs, where the compressive stress of the cycle is usually large compared to the tensile stress. Therefore, a conservative approximation of the fatigue performance that covers a wide range of applications can be obtained from the tests. The applied load ranges are between 2 to 3 kN and differ between various specimens. The loading jack position varies slightly between the specimens. Note that the roller plate clamping may induce an unknown level of constraint. The boundary conditions of the deck plate, i.e., fully support or clamping at the upper and lower edges,

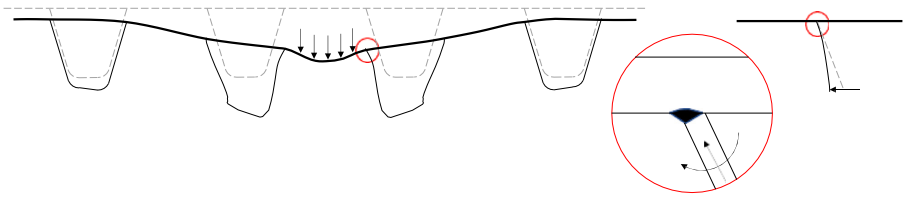

Fig. 6. Crack driving force for details C2a and C2b due to local distortion of the stiffener web.

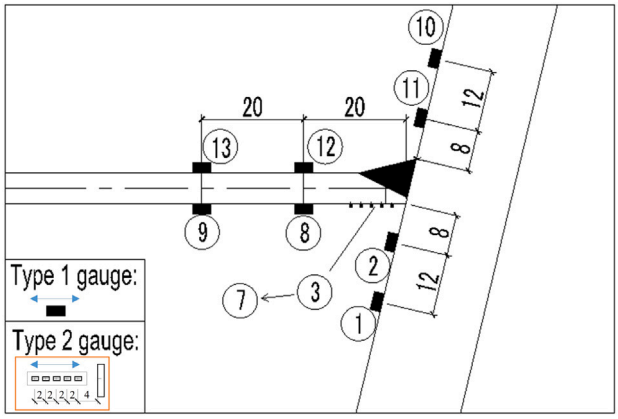

Fig. 7. Arrangement of strain gauges at the centre of the specimen (unit: mm).

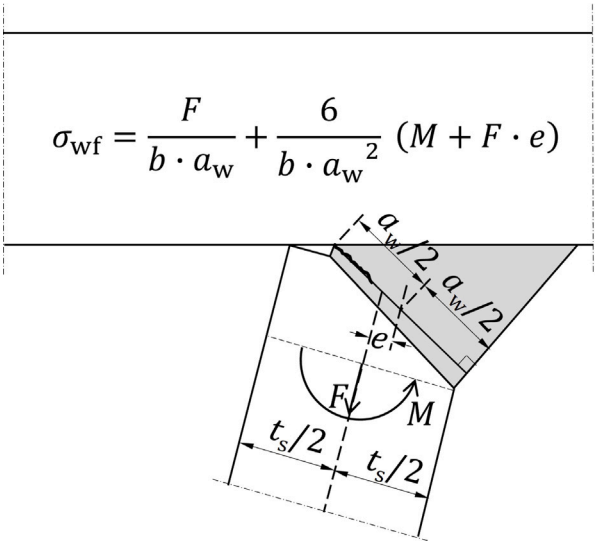

Fig. 8. Illustration in TS [5] for defining the structural stress in single-sided partial penetration welded connections.

do not affect the stress distribution in the region of interest for details C2a and C2b. The load application in the test – a force applied to the stiffener web – deviates from the load applied to the deck plate in a real OBD. However, the crack driving force for details C2a and C2b is the local distortion of the web [10,26]. Distortion is induced in both the real situation and the test, Fig. 6, and the local crack driving forces can be determined for both cases, as explained in Section 2.3.

Electric resistance strain gauges are attached to the stiffener and the deck plate in the middle of the specimen's width, see Fig. 7. Two types of strain gauges are attached, namely, a single gauge (Type 1) and a five-in-a-row gauge with a distance of 2 mm in between (Type 2). Type 1 gauges with the label numbers 8, 9, 12, and 13 are placed at the bottom and the top of the stiffener with distances of 20 mm and 40 mm from the weld root. Type 1 gauges with the label numbers 1, 2, 10 and 11 are placed at the bottom of the deck plate with distances of 8 mm and 20 mm from the weld root or weld toe. Type 2 gauges are attached at the root side of the stiffener, with the first gauge positioned 4 mm away from the weld root. All gauges are positioned to measure the strains perpendicular to the weld direction.

2.3. Stress calculation

Eq. (2) gives the hot spot stress for the weld toe (detail C2a) using the surface extrapolation approach as applied in the current paper where t_s is the thickness of stiffener. The stress ranges are calculated assuming an uni-axial stress state as a conservative reference.

$$\Delta\sigma_{hs} = 1.5 \cdot \Delta\sigma_{0.5t_s} - 0.5 \cdot \Delta\sigma_{1.5t_s} \tag{2}$$

Eq. (3) gives the calculation of the structural stress of the single-sided partial penetration welded connections in TS [5], detail C2b as shown in Fig. 8. The stress value is a function of the axial force range ΔF and the bending moment range ΔM. The additional bending moment caused by the eccentric axial force is also accounted for. The validation of Eq. (3) is presented in [2].

$$\Delta\sigma_{wf} = \frac{\Delta F}{b \cdot a_w} + \frac{6}{b \cdot a_w^2}(\Delta M + \Delta F \cdot e) \tag{3}$$

The stress ranges at the weld root $\Delta\sigma_{wf}$ of the specimens in the current paper can be calculated using Eqs. (4) to (6).

$$\Delta\sigma_{wf} = \Delta M \ \frac{6}{b \cdot a_w^2} \tag{4}$$

where

$$\Delta M = 2\Delta M_1 - \Delta M_2 \tag{5}$$

$$\Delta M_{1(2)} = \frac{b \cdot t_s^2}{6} \ E \ \Delta\varepsilon_{1(2)} \tag{6}$$

The bending moment range at the weld root, ΔM, is calculated by extrapolating the bending moment ranges at 20 mm (ΔM_1) and at 40 mm (ΔM_2) away from the weld root. These bending moment ranges are calculated from the measured strain ranges $\Delta\varepsilon_{1(2)}$ from Type 1 gauges 8 and 9. E is the Elastic modulus of steel, for which a value of 210 GPa is assumed. The variables a_w and b are the thickness of the weld and the specimen width, respectively. The eccentricity, e, can be calculated using a_w and t_s as shown in Fig. 8. The weld throat thickness, a_w, is taken as the average value of twenty measured fracture surfaces at an equal intermediate distance, determined after the complete failure of each tested specimen as summarized in Table 3.

2.4. Experimental results and fatigue resistances

Two definitions of fatigue life are commonly used in the literature to evaluate the data of details in OBDs. The first approach defines the number of cycles to failure using a change of strain range in the strain gauge closest to the fatigue crack initiation position [1,25,38,39]. However, this definition is sensitive to the distance between the crack initiation position and the closest strain gauge, and to the stress gradient. The second approach defines the number of cycles to failure by

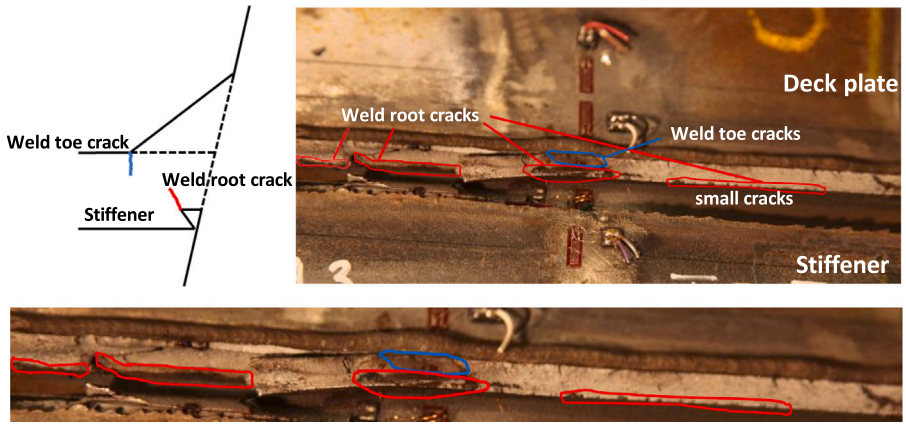

Fig. 9. Fracture surface of the specimen S2T3.

the specimen rupture. This definition is often used in the experiments using small-scale specimens and can only be used if crack arrest does not occur. For the tested specimens presented in the current paper, strain gauges are only placed in the middle of the specimens while the crack initiation positions may occur at other positions. The tests are terminated when the specimens are ruptured, except for the run-outs if rupture does not take place after approximately 10 million cycles. The second approach is therefore employed for the definition of fatigue life.

Table 3 summarizes the fatigue test results. Various load ranges are applied as required for statistical analysis. The structural stress ranges at the weld throat $\Delta\sigma_{wf}$ range between 146 and 359 MPa. The hot spot stress ranges $\Delta\sigma_{hs}$, calculated by Eq. (2) with the detailed description in Section 3, range between 242 and 381 MPa. Because the specimen S1T3 is a run-out, the fracture surface cannot be measured and $\Delta\sigma_{wf}$ is therefore not available. The strain gauges malfunctioned in the tests of S1T3 and S2T3 (with $\Delta\sigma_{hs(/wf)}$ marked by "a"). The average stress $\Delta\sigma_{hs(/wf)}$ normalized to one kilonewton of the other specimens in the corresponding detail group are linearly scaled with the applied forces for these two specimens. Fig. 9 shows a typical example of the observed failure modes. Cracks initiating from the weld toe of the stiffener and propagating through the stiffener (type C2a) are observed near the middle of the specimens. Cracks initiating from the weld root and growing through the weld (type C2b) are observed near the middle and the edges of the specimens. Table 3 lists the cracks observed in the fractured specimens.

The number of cycles to failure, N_f, ranges between 0.34 and 5.31 million. A test result is classified as "failure A" if N_f does not exceed 5 million for weld toe cracks or 10 million for weld root cracks. These threshold values for N_f correspond to the assumed constant amplitude fatigue limits in the upcoming second generation of Eurocode on fatigue of steel structures, EN1993-1-9 [10]. Fractured specimens with N_f beyond the above-mentioned limits are classified as "failure B". Only data of "failure A" are used in the statistical analysis of the fatigue resistance with a fixed slope, in line with [40,41]. Specimens showing signs of both weld toe and root failures are incorporated in the statistical evaluation of both positions. Specimens with only the weld toe failure are considered as run-outs for the weld root failure and vice versa. Similar to "failure B" test data, run-outs are disregarded in the statistical evaluation.

Figs. 10 to 11 show the results of the statistical analyses, using the Basquin relation $log(N_f) = a_N - m \times log(\Delta\sigma_{hs(/wf)})$ and assuming a fixed slope $m = 3$. The fatigue resistance is expressed as the stress range at which two million cycles to failure is obtained, with exceedance probabilities P_s = 95%, 50%, 5%. The 95% value is further referred to as the characteristic fatigue resistance $\Delta\sigma_C$, defined in (pr)EN 1993-1-9 [9,10] and TS [5], following the statistical analysis described in [40,41]. A relatively high fatigue resistance with a narrow scatter band ($\Delta\sigma_C$ = 272 MPa with the standard deviation s = 0.09) is observed for detail C2a of S1 in Fig. 10a, as compared to S2 ($\Delta\sigma_C$ = 159 MPa with the standard deviation s = 0.14), Fig. 10b. Fig. 11 shows the results of detail C2b. S2 gives a significantly lower fatigue resistance ($\Delta\sigma_C$ = 106 MPa with the standard deviation s = 0.22) as compared to S1 ($\Delta\sigma_C$ = 158 MPa with the standard deviation s = 0.29), indicating a better fatigue performance of automatic welded connections for detail C2b. Note that both weld toe and root failures occur; the fact that the fatigue resistance values are different is caused by the different stress definitions for the two details.

Table 3
Summary of the fatigue test results.

ID	ΔF [kN]	a_w [mm]	$\Delta\sigma_{wf}$ [MPa]	$\Delta\sigma_{hs}$ [MPa]	N_f	Final crack surface observation
S1T1	2.00	8.00	156	266	5 311 008	Root+Toe
S1T2	1.99	6.10	282	269	4 462 209	Root+Toe
S1T3	1.99	–	203[a]	242[a]	9 577 675	Run-out
S1T4	2.26	6.25	315	321	1 505 820	Toe
S1T5	2.44	6.10	306	306	2 204 211	Root+Toe
S1T6	2.41	7.56	209	311	2 836 078	Root
S1T7	2.93	6.75	296	349	1 278 523	Toe
S1T8	2.93	7.48	207	321	2 100 102	Root+Toe
S1T9	2.94	7.01	276	346	1 377 320	Root+Toe
Avg.		6.91				
S2T1	2.04	6.93	215	278	1 592 180	Root+Toe
S2T2	2.04	7.61	181	261	1 140 391	Root+Toe
S2T3	1.99	6.99	199[a]	254[a]	1 610 468	Root+Toe
S2T4	1.99	8.01	146	251	1 037 337	Root
S2T5	2.64	6.10	359	356	345 712	Toe
S2T6	2.51	6.10	332	315	490 183	Toe
S2T7	2.52	6.84	253	317	358 240	Root+Toe
S2T8	2.94	6.76	293	363	370 673	Root+Toe
S2T9	2.93	7.32	242	349	400 696	Root+Toe
S2T10	2.94	7.33	271	381	341 855	Root+Toe
Avg.		7.00				

Note:
SXTY: represents the Series **X**, Test **Y**.
[a] Value calculated using the average $\Delta\sigma$ from the corresponding detail group.

2.5. Additional experimental results in the literature

2.5.1. Ya (2009)

A similar experimental setup and specimen geometries were used at Nagoya University by Ya [29], but using thinner deck plates and automatic weld only. The specimens were 500 mm wide with a 200 mm long stiffener and a 315 mm long deck plate. The specimens were sorted into six groups with deck plate thicknesses of 12, 14, and 16 mm, stiffener thicknesses of 6 and 8 mm, and weld penetration ratios of 30%, 75%, 80%, and melt-through. Only the results with weld penetration ratios from 75% to 80% from [29] are used in the current paper. The

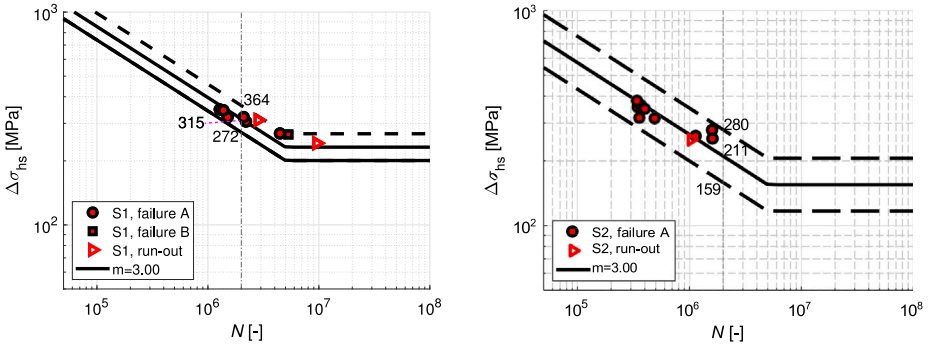

(a) S1, s = 0.09 (b) S2, s = 0.14

Fig. 10. Statistical analysis for detail C2a.

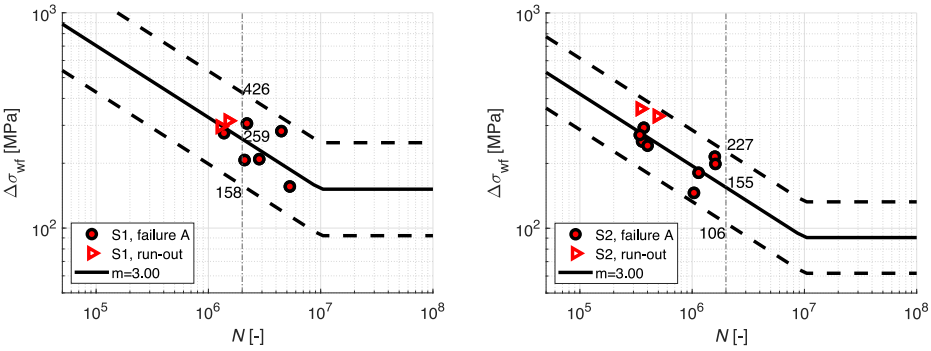

(a) S1, s = 0.29 (b) S2, s = 0.22

Fig. 11. Statistical analysis for detail C2b.

tests were carried out with a load ratio of $R = -1$. Copper wires 0.04 mm in diameter were placed at the weld surface and the weld toe. The tests were stopped when the wires were cut due to the cracking of the specimens.

A statistical evaluation of automatic welded connections is carried out on the joint database, consisting of the experimental results of Ya (2009) [29] and the ones of Section 2.4, assuming a fixed slope parameter of $m = 3$. Fig. 12 shows the results. The characteristic values of fatigue resistance are 276 MPa and 142 MPa for details C2a and C2b, respectively. The joint database's fatigue resistances are almost equal to that of the separate database of detail C2a, see Fig. 10a. On the other hand, the joint database gives lower values (with $P_s = 95\%$ or 50%) for detail C2b. The corresponding standard deviation increases from 0.29 (Fig. 11a) to 0.33 (Fig. 12b).

2.5.2. Yuan (2011) and Bruls (1991)

Fig. 13 shows the analysis adding the results from Yuan [24] and Bruls [30]. The stress in [24] was calculated by the FE method. Yuan [24] carried out fatigue tests with a single stiffener-to-deck assembly. The stiffener was centrally loaded with $R = 0$ or -1 (only the results with $R = -1$ are used in the current paper) and the deck plate was supported at its edges (at semi-distance between the closed stiffeners). The specimens failed from the weld toe (type C2a). Bruls [30] carried out similar tests. But the stiffener was positioned eccentrically and the load was exerted on the deck plate, with $-1 \le R \le 0$. The specimens failed from the weld root (type C2b). The specimens with the penetration ratios range $75\% \le \text{PJP} < 100\%$ are used in the current paper. Both series used automatic welding procedures.

Fig. 13 shows the statistical evaluation results of the joint database. The characteristic values $\Delta\sigma_C$ is 158 MPa with the s equal to 0.32 for detail C2a. A higher $\Delta\sigma_C$ = 158 MPa with a slightly smaller s = 0.30 is obtained compared with the values in Fig. 12b for detail C2b. Combining the data, the resulting characteristic values for details C2a and C2b are shown in Table 4.

Table 4
Fatigue resistances derived from all tests.

Detail	Stress	Weld procedure	Characteristic value $\Delta\sigma_C$
C2a	Eq. (2)	Automatic & manual	158 MPa (Fig. 13a)
C2b	Eq. (3)	Automatic Manual	158 MPa (Fig. 13b) 106 MPa (Fig. 11b)

3. Finite element modelling

Section 2 experimentally evaluates the fatigue behaviour of details C2a and C2b. Section 3 describes the FE study of details C2a and C2b. Plane strain FE models of the current specimens are built using the commercial software Abaqus 2019 [42]. Displacement and rotation constraints, UX = UY = URZ = 0, are used to the top of the deck plate over its entire surface, see Fig. 14. Eight-node plane strain elements with reduced integration, type CPE8R, are employed with element sizes of approximately 0.5×0.5 mm^2 [42]. The weld penetration ratio equals 75%, i.e., the specified (minimum) ratio of the specimens. A possible contact between the stiffener edge and the deck plate is not modelled, as expressed by a 0.01 mm gap as shown in Fig. 14. Further, the Elastic modulus $E = 210$ GPa and Poisson's ratio $\nu = 0.3$.

The stiffener edge is free to rotate in the FE model, and by a calibration procedure the loading position is determined such, that the computed normal strains are equal to the measured ones. The calibration results in a load position 37.5 mm away from the free stiffener edge. The shear strains are verified to be negligibly small in

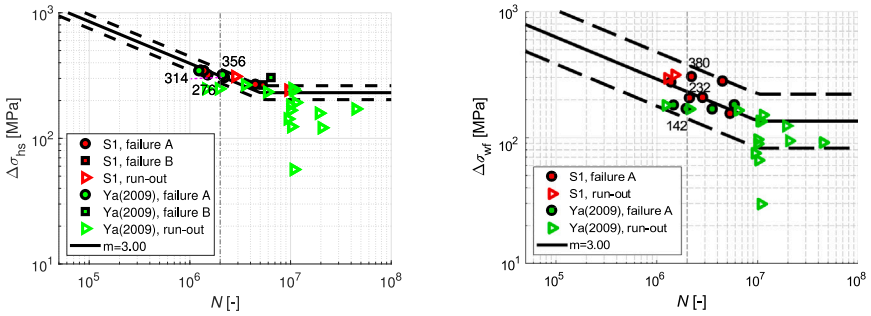

(a) detail C2a, s = 0.08 (b) detail C2b, s = 0.33

Fig. 12. Statistical analysis for automatic welding, including S1 and Ya (2009) [29].

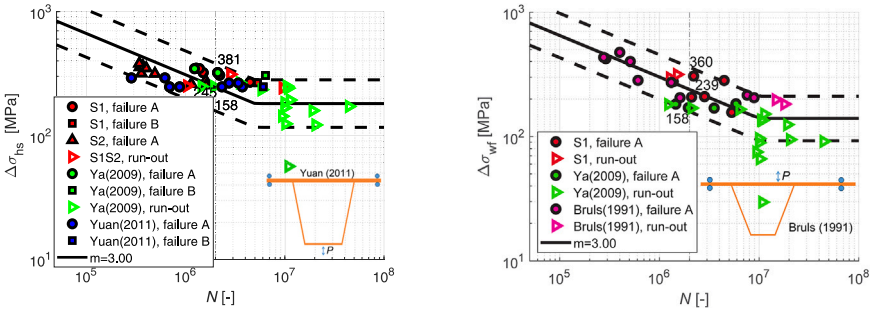

(a) detail C2a, s = 0.32 (b) detail C2b, s = 0.30

Fig. 13. Statistical analysis for automatic welding, including data in the literature [24,29,30].

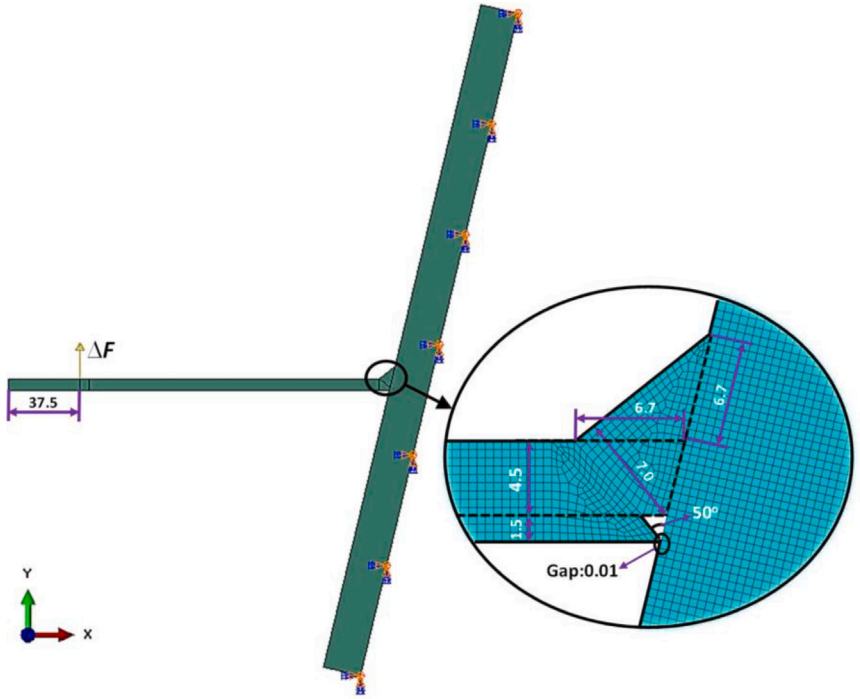

Fig. 14. Sketch of the FE model (unit: mm).

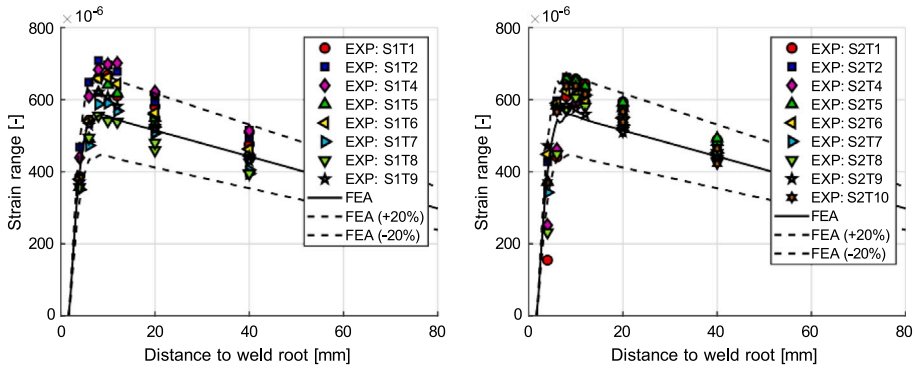

(a) S1 (b) S2

Fig. 15. Comparison of experimentally measured and FE calculated strain ranges at the bottom (inner) side of the stiffener, normalized to a load range of 5 N/mm.

the studied cases. $\sigma_{hs} = -131$ MPa and $\sigma_{wf} = 100$ MPa are obtained accordingly, normalized to a unit load of 1 kN (equivalent to 5 N/mm).

Fig. 15 shows a comparison of the strains between the FE computed (FEA) and the experimentally measured (EXP) in which a scatter of strains between the measurements is evident. Almost all measured strains are within the bounds set by ±20% offset from the FEA. In both the experimental study and FE simulation, the strain ranges increase at the bottom side of the stiffener when approaching the welded connection, followed by a significant decrease very close to the weld. This decrease starts from the position of approximately 10 mm from the weld root. It is caused by the lack of penetration and the increase in cross-section thickness. The weld toe is, therefore, assumed at a distance of 10 mm from the weld root in calculating $\Delta\sigma_{hs}$ with Eq. (2).

4. Parametric analysis using local approaches

4.1. Effective notch stress method

The ENS method is developed to evaluate the fatigue behaviour of the weld toe and root by the FE method using linear elastic material [6]. A fictitious notch with a radius R_{ref} is adopted at weld toe and root to avoid numerical stress singularities. Either the maximum principal stress or the von Mises stress on the curve of the notch radius is referred to as the effective notch stress. The maximum principal stress criterion is better than the von Mises stress criterion for the proportional loading [43]. The effective notch radii R_{ref} and the characteristic fatigue resistance $\Delta\sigma_C$ depend on the plate thickness t [6]:

- for $t \geq 5$ mm, $R_{ref} = 1.00$ mm and $\Delta\sigma_C = 225$ MPa;
- for $t < 5$ mm, $R_{ref} = 0.05$ mm and $\Delta\sigma_C = 630$ MPa;

where the values for $\Delta\sigma_C$ are valid for the principal stress, and they are defined at a survival probability of 97.7%. This method was applied to analyse the fatigue behaviour of large-scale welded joints and under multi-axial stress states [44,45]. The ENS method enables estimating the effect on the fatigue resistance of local geometric characteristics. In the current paper, the ENS method is used to study the effect of weld penetration ratios of 25%, 50%, 75%, 87.5%, and 100%.

Fig. 16a gives a close-up of the welded connection in the FE model with a weld penetration ratio of 50% as an example. The predefined penetration ratio is calculated as t_p/t_s where t_p and t_s are the thicknesses of the penetration part and the stiffener, respectively. The element type, the entire (global) geometry, the load and the boundary conditions are the same as in Section 3. Effective notch radii are applied at all four possible crack initiation locations. The notches for crack locations C2b and C1b coincide in the case of penetration ratios of 75%, 87.5%, and 100%. They are then merged, and in addition, additional simulations are performed with the models with an effective notch radius of $R_{ref} = 0.05$ mm, as shown in Fig. 16b, even though the plate thicknesses are larger than 5 mm.

Figs. 17 and 18 show contour plots of the maximum principal stresses in absolute values in the vicinity of the welded connections with 1.00 mm and 0.05 mm radii notches under a load of 5 N/mm in the positive y-direction, respectively. Either detail C2a or C2b is critical according to the FEA, depending on the penetration ratio. These findings agree well with the observed fracture locations in the experiments, where both C2a and C2b types cracks, are observed. The penetration ratio appears to have a significant effect on the principal stress for both details C2a and C2b. Fig. 17 shows that the maximum principal stress at detail C2b with a penetration ratio of 25% is approximately 2.8 times that of 50% and approximately 5.5 times that of 75% penetration ratio. With 87.5% and 100% penetration ratios, the values are 0.82 and 0.64 times that of 75%, respectively.

A similar trend between minimum principal stress (corresponding to the maximum absolute value in cyclic loading) and penetration ratios from 25% to 75% is found for detail C2a. The value then keeps constant till 100% penetration ratio. When the notch radius $R_{ref} = 0.05$ mm is employed as shown in Fig. 18, the maximum principal stresses are 2.0 to 2.4 and 2.5 to 3.4 times larger compared to $R_{ref} = 1.00$ mm for details C2a and C2b, respectively. Note that the ratio in the fatigue resistance in [6] is 2.8.

Figs. 19 and 20 give the maximum principal stress (in absolute value) distribution along the notches. The angles at which the maximum principal stresses are located depend slightly on penetration ratios. The results are summarized in Table 5 where the absolute maximum values are shown in bold. Detail C2b is critical for penetration ratios between 25% and 50%, and detail C2a for penetration ratios between 87.5% and 100%. For the case with a 75% penetration ratio, the maximum ENS for a radius of 0.05 mm is at C2b, while it is at C2a for $R_{ref} = 1.00$ mm.

4.2. Averaged strain energy density factor method

Plane strain FE models similar to Fig. 16 are built assuming the notches are replaced by a local dense meshed area with element sizes of approximately 0.02×0.02 mm^2 ([46] illustrates that the SED method is not sensitive to element size). The SED averaged over the region enclosed by the circle with $R_{ref} = 0.28$ mm is calculated as the summed SED over that region divided by its area. The characteristic fatigue resistance and the slope parameter can be found in Section 1.

Table 5 gives the SED of the aforementioned weld penetration ratios. The averaged SED for the weld root cracks (types C1b and C2b) reduces significantly with increasing penetration ratios from 25% to 75%, and it reduces slightly for penetration ratios increasing from 75% to 100%. For the weld toe crack (type C2a), the SED reduces significantly for a penetration ratio increasing from 25% to 50%, and

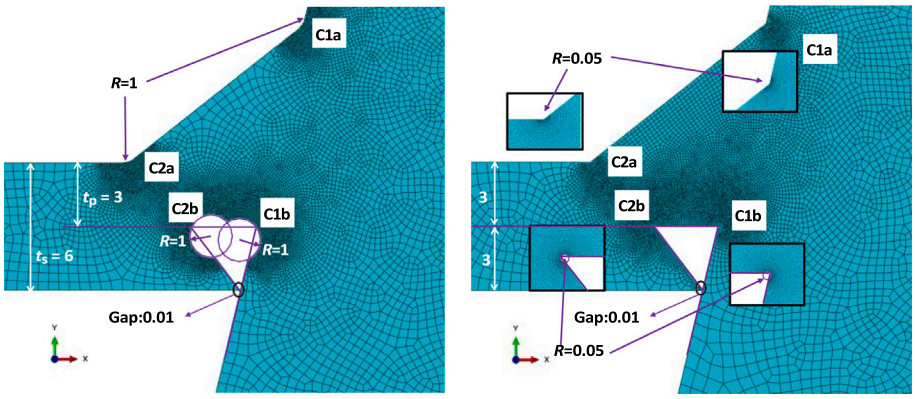

(a) R_{ref} = 1.00 mm (b) R_{ref} = 0.05 mm

Fig. 16. Details of the FE models for the ENS calculation with a weld penetration ratio of 50%, (unit: mm).

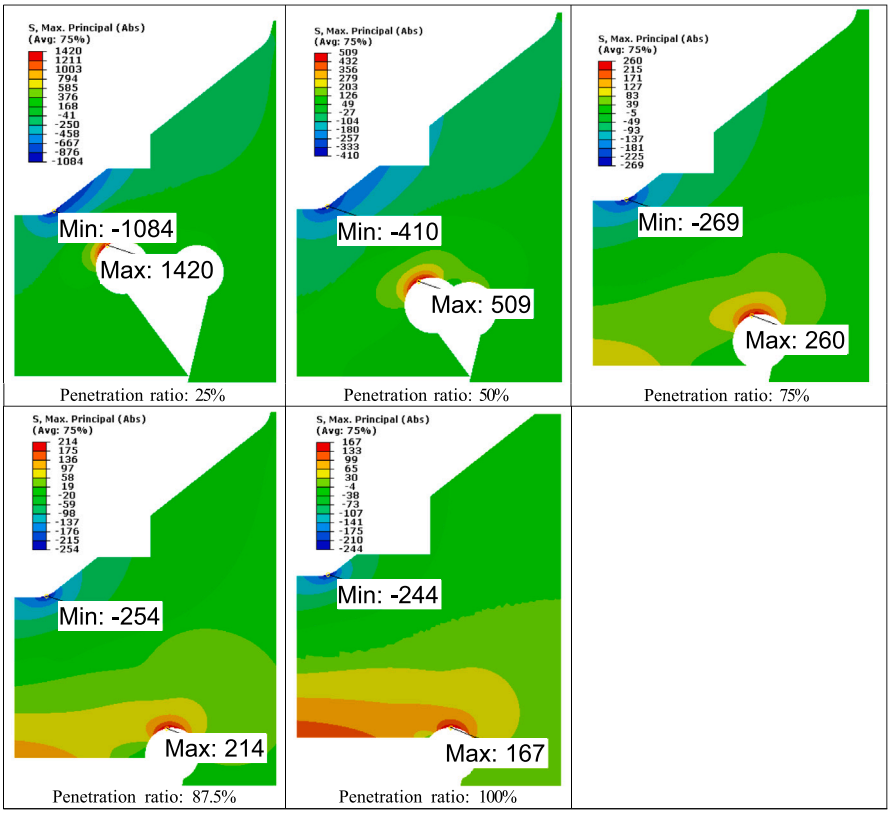

Fig. 17. Principal stress contour plot of the welded connections with notch R_{ref} = 1.00 mm, under a load of 5 N/mm in the positive *y*-direction (unit: MPa).

Table 5
ENS and SED with different penetration ratios under a load of 5 N/mm in the positive y-direction with the highest absolute (decisive) values are marked in bold (unit: MPa or N mm/mm^3).

Penetration ratio	ENS R_{ref} = 1.00 mm				ENS R_{ref} = 0.05 mm				SED ($\times 10^{-4}$) R_{ref} = 0.28 mm			
	C1b	C2b	C2a	C1a	C1b	C2b	C2a	C1a	C1b	C2b	C2a	C1a
25.0%	385	**1420**	−1084	−70	833	**4461**	−2121	−150	744	**15770**	9501	54
50.0%	221	**509**	−410	−52	639	**1722**	−922	−97	408	**2380**	1819	30
75.0%	260	260	**−269**	−41	530	**811**	−638	−90	279	555	**874**	19
87.5%		214	**−254**	−35	496	535	**−593**	−80	261	264	**762**	15
100.0%		167	**−244**	−31		430	**−583**	−69		181	**729**	11

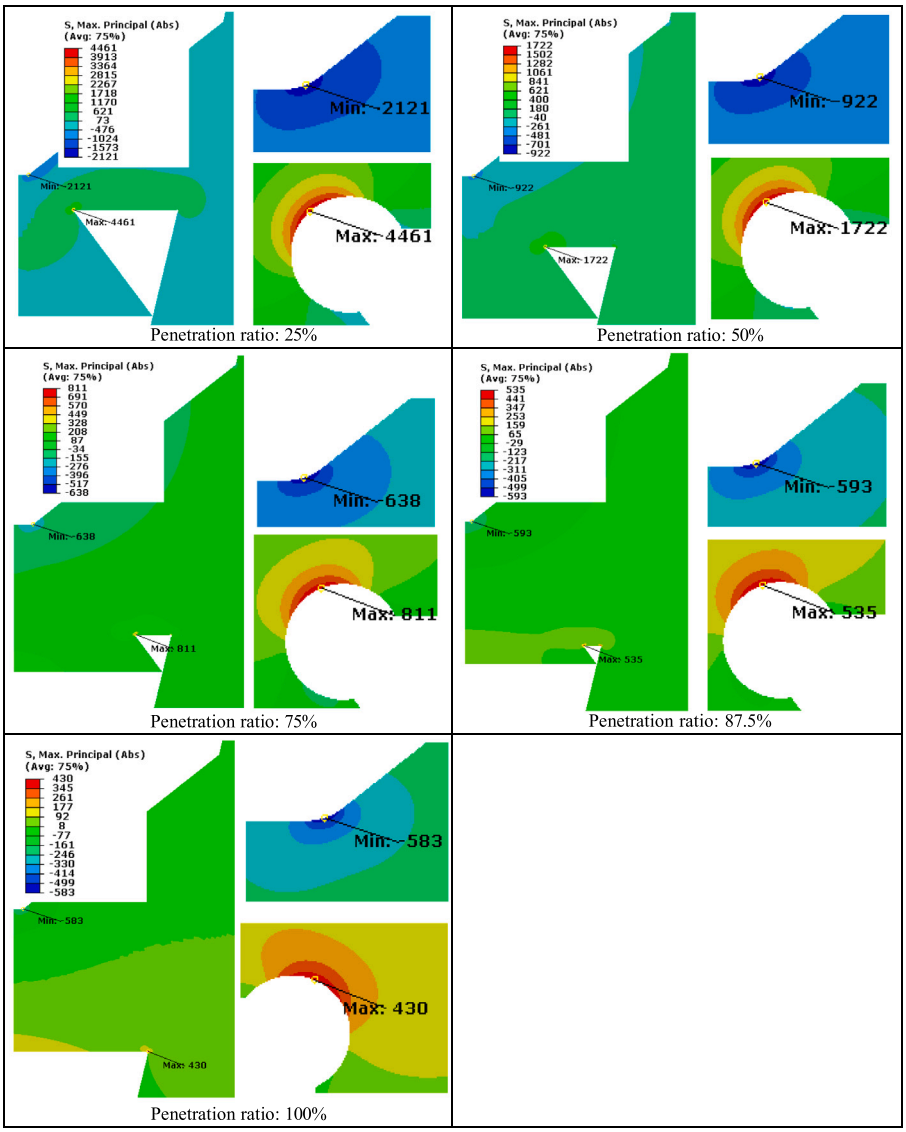

Fig. 18. Principal stress contour plot of the welded connections with notch $R_{ref} = 0.05$ mm under a load of 5 N/mm in the positive y-direction (unit: MPa).

then it reduces slightly for further increasing penetration ratios. The critical position shifts from detail C2b to detail C2a for weld penetration ratios exceeding 75%. The predicted critical positions are the same as with the ENS with $R_{ref} = 1.00$ mm.

4.3. Fracture mechanics method

The fracture mechanics method is an attractive approach to analyse the fatigue crack propagation behaviour [6,47]. In a welded component, the flaws caused by the manufacturing and/or fabrication can be treated as initial cracks, especially in incomplete penetration welds [48]. In that case, the crack initiation life can be ignored, and the crack propagation life is a reasonable estimate of the total life.

In the current paper, crack propagation is simulated using the XFEM, assuming a plane strain condition for the sake of numerical convenience. The XFEM module in Abaqus is employed using the Virtual Crack Closure Technique (VCCT) [42], with phantom nodes to simulate discontinuities in the enriched element. The enriched element is released with zero constraints and zero stiffness after cracking.

4.3.1. Mesh and initial crack

Initial cracks with a depth of $a_i = 0.1$ mm are inserted at the positions as shown in Fig. 21 to study detail C2a or C2b. The location and the angle of the initial crack follow the maximum principal stress location and the initial angle is obtained in the ENS simulation with $R_{ref} = 0.05$ mm in Fig. 20. An exception is the model for simulating a C2b type crack with 100% penetration. The initial crack is applied parallel to the edge of the deck plate (corresponding to the angle 77° in Fig. 20a). Different types of elements and mesh sizes are applied for the region of interest (grey colour sub-model in Fig. 21) and the part further away from the welded connection (red colour). These two parts are connected by tie constraints, which implies that the edges have the same displacement [42]. The element size of the sub-model is, on average, 0.1×0.1 mm^2 with a denser mesh close to the initial crack location. The element size in the global part is approximately 0.5×0.5 mm^2. First-order enriched elements with reduced integration of type CPE4R are applied in the sub-model, and regular second-order elements with reduced integration of type CPE8R are applied in the remaining part of the model [42].

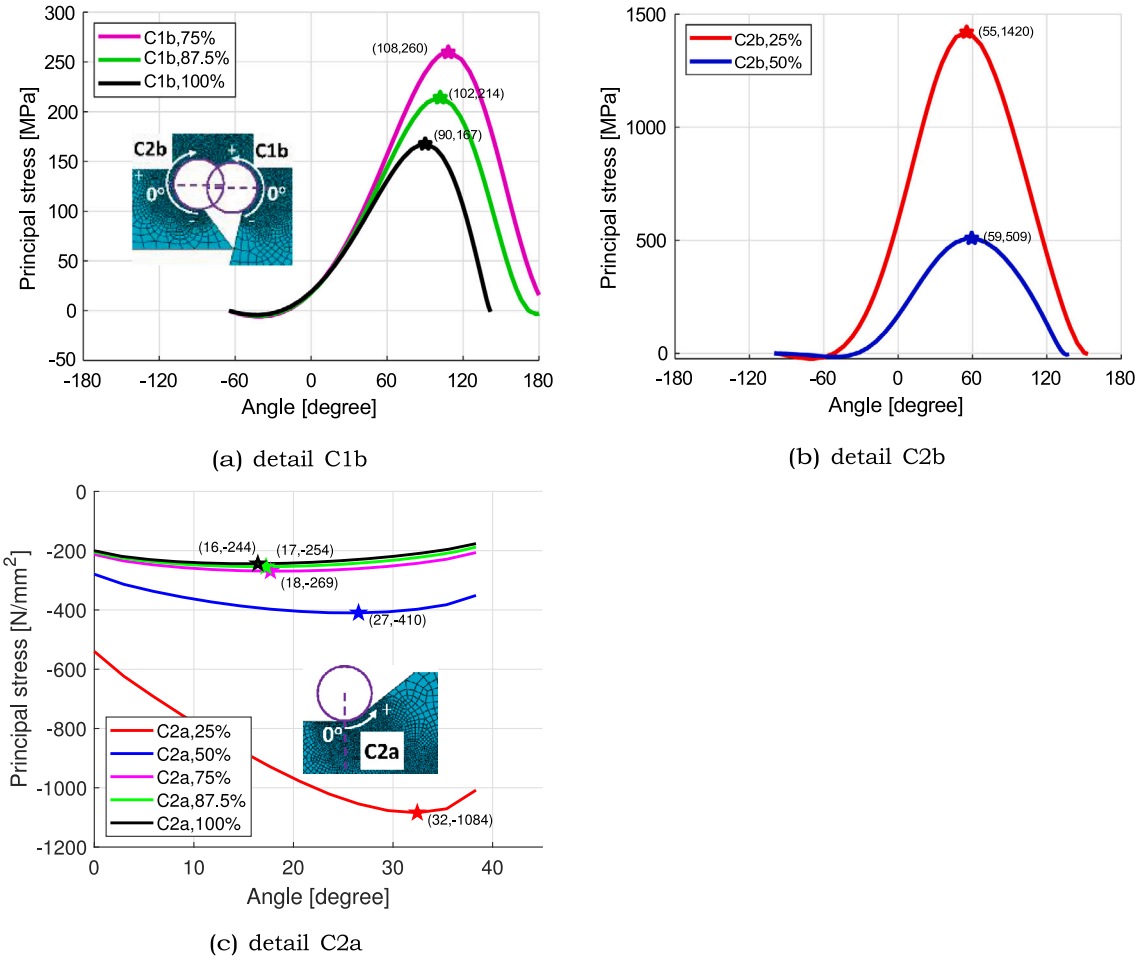

Fig. 19. Principal stress distribution along the notches with $R_{\text{ref}} = 1.00$ mm under a load of 5 N/mm in the positive y-direction.

4.3.2. Crack propagation

In the calculation, the stress intensity factor ranges are above the assumed threshold value, $\Delta K_{\text{th}} = 63\ \text{N/mm}^{1.5}$ [31], due to the high load ranges applied in FEA according to the experimental results. The Paris' equation is therefore used to relate the stress intensity factor range to the crack extension per cycle:

$$\frac{da}{dN} = C \cdot \left(\Delta K_{\text{eq}}\right)^m \tag{7}$$

$$\Delta K_{\text{eq}} = \sqrt{\Delta K_1^2 + \Delta K_2^2} \tag{8}$$

$$\Delta K_{\text{i}} = K_{\text{i,max}} - K_{\text{i,min}},\ i = 1, 2 \tag{9}$$

The following material parameters are used based on the IIW recommendations [31]:

- $C = 5.21 \times 10^{-13}$ (units: N and mm) for a probability of survival of 97.7%.
- m is 3.

The subroutine "UMIXMODEFATIGUE" is used to define the crack propagation law in Abaqus [42]. It uses the strain energy release rate G instead of the stress intensity factor:

$$\frac{da}{dN} = C_3 \cdot \left(\Delta G_{\text{eq}}\right)^{c_4} \tag{10}$$

$$G_{\text{i}} = K_{\text{i}}^2 / E' \tag{11}$$

where:

$$E' = \frac{E}{1-\nu^2},\ \text{plane strain} \tag{12}$$

$$\Delta G_{\text{eq}} = \Delta G_{\text{I}} + \Delta G_{\text{II}} \tag{13}$$

The load ratio $R = -1$ is applied, same as in the experiments. Two simulations are carried out, which may imply an upper- and a lower bound of reality:

- Fracture Mechanics 1 (FM 1): The cracked part is assumed to be closed and does not propagate in the compressive semi-cycle.
- Fracture Mechanics 2 (FM 2): The cracked part remains open during loading. The complete cycle is effective in crack propagation.

A more detailed analysis including crack closure or the effective stress intensity factor ranges [17] is not carried out because of large uncertainties of the welding-induced residual stress. The Paris' equation constant C for high stress ratio situations is employed. The crack increment applied in the simulation is controlled up to 0.03 mm at maximum. The Maximum Tangential Stress criterion is employed for the crack propagation direction [42].

4.3.3. Results of the XFEM simulation

Fig. 22 shows the predicted crack paths of the XFEM simulations for weld penetration ratios of 75%, 87.5% and 100%. The crack propagates to the bottom (inner) side of the stiffener (Fig. 22a) and the weld surface (Fig. 22b) for the weld toe and root cracks, respectively. The predicted fatigue lives under the applied load with the maximum value equal to 5 N/mm (FM 1) are shown in Fig. 23. The predicted fatigue lives of detail C2a are independent of the penetration ratios considered, while that of detail C2b depends on the penetration ratios. These findings are qualitatively in agreement with the results of the ENS analyses.

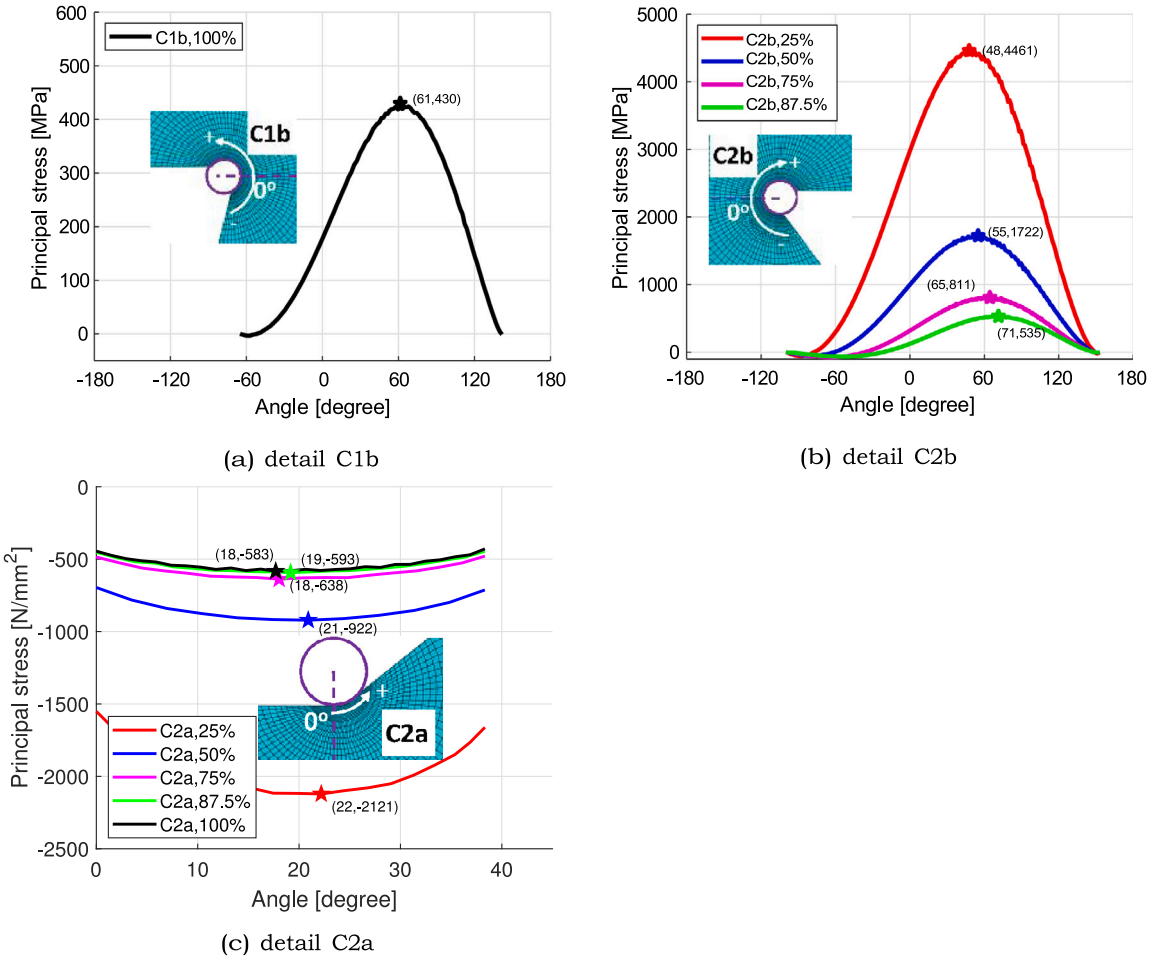

Fig. 20. Principal stress distribution along the notches with $R_{ref} = 0.05$ mm under a load of 5 N/mm in the positive y-direction.

The predicted fatigue lives of the two cracks are approximately equal for the case with a penetration ratio of 75%, which are also observed with the ENS with $R_{ref} = 1.00$ mm. Shorter lives are predicted for detail C2a than for detail C2b in case of higher penetration ratios, again in line with the ENS analyses.

5. Comparison of the different fatigue assessment methods

A comparison between the experimentally obtained fatigue resistances of the specimens in Section 2 and the predicted resistances according to the local methods in Section 4 is presented in this section. The weld throat thicknesses of detail C2b in the FE models are obtained by the measurement of the distance between the crack initiation position and the fracture surface in the models. The corresponding $\Delta\sigma_{wf}$ in the numerical simulation is calculated under the plane strain condition.

Fig. 24 shows the values for $\Delta\sigma_C$, calculated by the local methods, with a 97.7% prediction bound, and the values determined by the fatigue tests in Section 2, with a 95% prediction bound, all at 2 million cycles. In addition to the commonly recommended $C = 5.21\times10^{-13}$, the value $C = 3.00\times10^{-13}$ is also used for the weld toe crack propagating into base material [31] and therefore included here.

FM 1 (assuming crack closure at the external compressive load) with $C = 3.00\times10^{-13}$ gives excellent predictions for detail C2a. The differences between the predicted resistances and experimentally obtained values in Section 2 are within 5% for penetration ratios of 75%, 87.5%, and 100%. The data for 100% penetration ratio are added for reasons of comparison; the experiments have a penetration ratio between 75% and 100%, but probably closer to the lower bound because melt-through

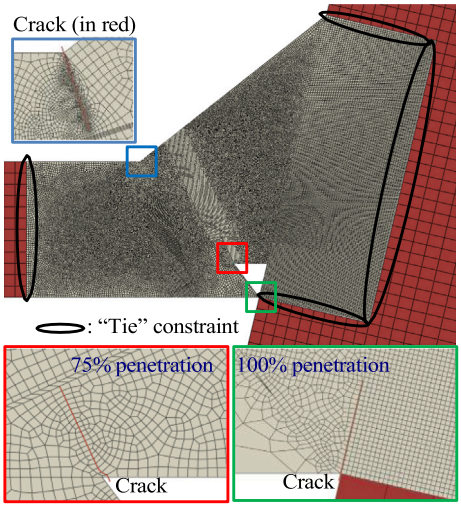

Fig. 21. Details of the initial cracks $a_i = 0.1$ mm inserted in the FE models (cracks presented as red wires). (For interpretation of the references to colour in this figure legend, the reader is referred to the web version of this article.)

was not allowed (see Section 2). For detail C2b and a penetration ratio of 75%, the FM 1 predictions are 13% conservative and 29% unconservative for automatic and manual welds, respectively. The imperfection in manual welded connections may be larger than $a_i = 0.1$ mm, resulting in a lower fatigue resistance experimentally obtained

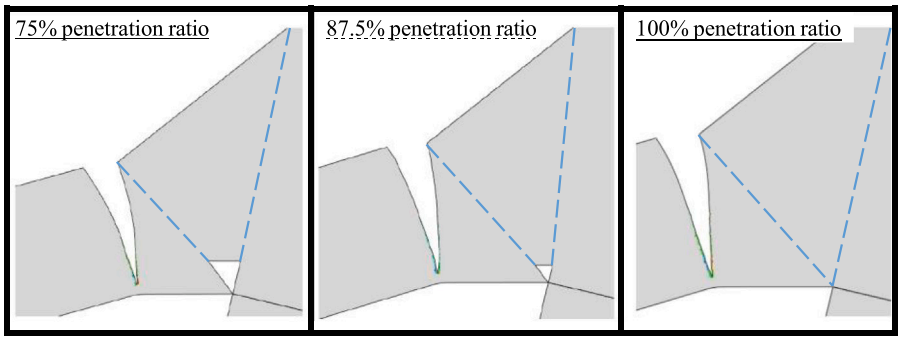

(a) detail C2a

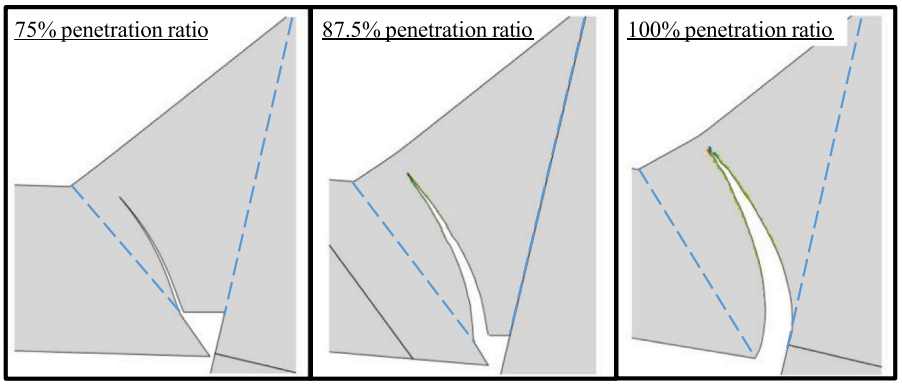

(b) detail C2b

Fig. 22. Typical crack propagation paths according to the XFEM simulations with penetration ratios: 75%, 87.5%, and 100%.

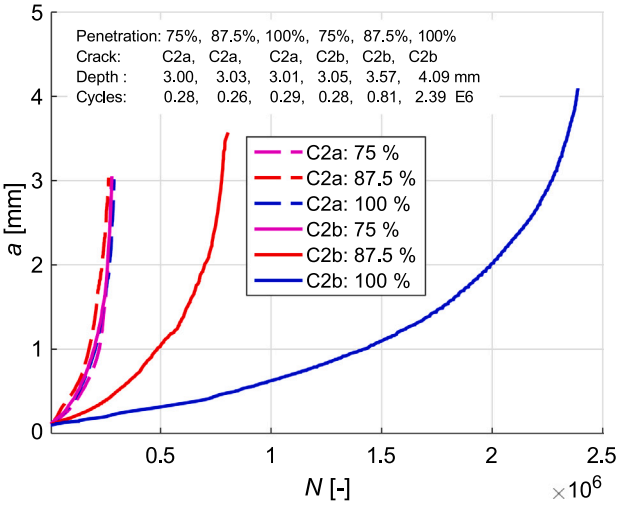

Fig. 23. Crack propagation simulation of FM 1, with $C = 5.21 \times 10^{-13}$, $m = 3$.

in Section 2 compared to the prediction. The data of the penetration ratios of 87.5% and 100% are added for comparison only, because the weld toe crack (type C2a) is predicted for such high penetration ratios. The assumption that the cracked part keeps open under compressive stress appears to underestimate the predictions for these for small-scale specimens under high load ranges. The ENS method gives conservative predictions for detail C2a, with lower values for $R_{\text{ref}} = 1.00$ mm than for $R_{\text{ref}} = 0.05$ mm. The SED method predicts lower characteristic fatigue resistances in the range of 151 to 165 MPa. The differences are within 5% of the experimental results. The resistance predictions for detail C2b show a significant increase with increasing weld penetration ratio. The SED, with a predicted characteristic fatigue resistance of up to 196 MPa, overestimates the resistances with factors of 1.2 and 1.8 for automatic and manual welding, respectively, assuming a penetration ratio of 75%. The overestimation is even larger for a penetration ratio of 87.5% or 100%, however, the methods predict the weld toe crack (type C2a) for these penetration ratios, so these values are added for comparison only. Nonetheless, the large over-prediction of the experimental fatigue resistances indicates that the SED is not suited for this type of crack.

6. Conclusions

Two series of fatigue tests on the stiffener-to-deck plate weld are conducted to investigate the crack initiating from the stiffener weld toe propagating into the base material (type C2a) and from the weld root propagating through the weld (type C2b). One series comprises automatic welded specimens, and the other series comprises manual welded specimens. All tests are carried out in bending with fully reversed load cycles. The weld penetration ratios of the specimens are between 75% and 100%. The following conclusions are drawn from the experimental investigation:

1. Both C2a and C2b types cracks are observed in the experiments. Hence, for the load condition and the penetration ratios applied, their fatigue performance is approximately equal, despite the different local geometries. Type C2b is more dominant in case of small penetration ratios and vice versa.
2. The automatic or manual welded connections have a characteristic fatigue resistance of 272 MPa ($s = 0.09$) or 159 MPa ($s = 0.14$), respectively, for detail C2a using the (structural) hot spot stress method. The characteristic fatigue resistance of detail C2b is 158 MPa ($s = 0.29$) or 106 MPa ($s = 0.22$) for automatic or manual welding, respectively, using the force equilibrium-based structural stress over the throat of the weld. Especially, the automatic welding procedure gives significantly higher characteristic fatigue resistances than the recommended values in [9–12] (ranging from 80 MPa to 100 MPa).

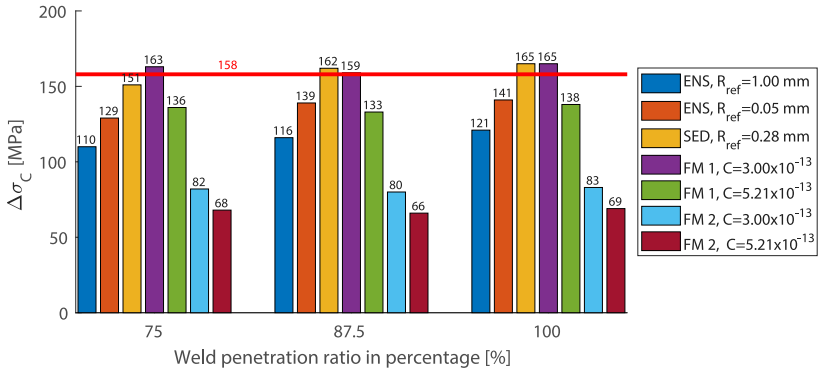

(a) detail C2a

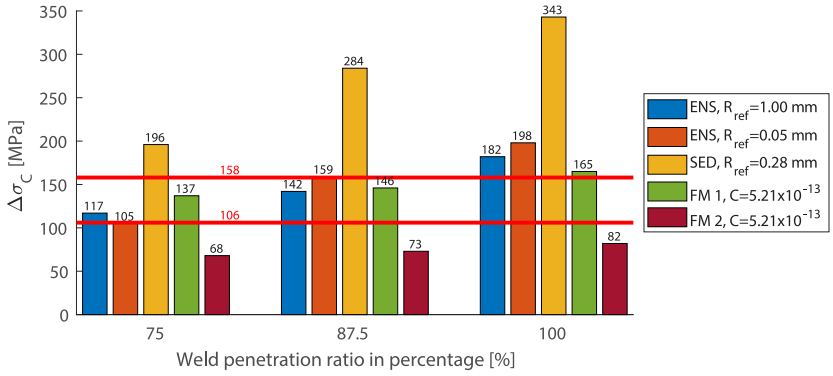

(b) detail C2b

Fig. 24. Comparison between the characteristic fatigue resistances calculated by the local methods (columns) and based on experiments (lines) for details C2a and C2b ($P_s = 95\%$ in the experiments, and $P_s = 97.7\%$ in the predictions).

3. Using the authors' own results and data in the literature, the recommended characteristic fatigue resistances are:
   - **160 MPa** for detail C2a with automatic or manual welding.
   - **140 MPa** for detail C2b with automatic welding.
   - **100 MPa** for detail C2b with manual welding.
4. No influence of the thickness of the deck plate ($12\ \text{mm} \le t_d \le 20\ \text{mm}$) on the characteristic fatigue resistances of details C2a and C2b is observed.

FE simulations based on the plane strain assumption are carried out using the effective notch stress, averaged strain energy density factor, and fracture mechanics methods, the latter assuming an initial crack depth of 0.1 mm. The effect of penetration ratios is assessed by these methods, bridging the existing knowledge of standard welded connections and the fatigue performance of welds in OBDs. An increase in weld penetration ratios from 25% to 75% significantly reduces the ENS and SED for both details C2a and C2b. For penetration ratios exceeding 75%, detail C2a is predicted as critical and no obvious change of the ENS and SED is observed.

When adopting the assumption that the crack is closed under external compressive stress, the FM simulation with an initial crack size of 0.1 mm gives excellent predictions for the fatigue resistance of detail C2a (automatic or manual welding) with an overestimation within 5% using $C = 3.00 \times 10^{-13}$ (unit: N and mm) and $m = 3$. The FM method considered in the paper using $C = 5.21 \times 10^{-13}$ (unit: N and mm) and $m = 3$ is useful for automatic welded C2b with penetration ratios from 75% to 100%. An initial crack size assumption of 0.1 mm may lead to a 29% overestimation of predicted resistance for manual welded C2b, assuming a penetration ratio of 75%. The SED method also gives good predictions for detail C2a, while the ENS method gives conservative predictions by up to 18% or 30% using the notch with radii of 0.05 mm or 1.00 mm, respectively. For detail C2b, assuming a penetration ratio of 75%, the resistance prediction with the ENS method is suitable for the manual weld procedure. The SED method is considered unsuited for this type of weld root crack (type C2b) because of the large overpredictions compared to the experimental results.

CRediT authorship contribution statement

Weijian Wu: Conceptualization, Data curation, Formal analysis, Investigation, Methodology, Validation, Visualization, Writing – original draft, Writing – review & editing. **Milan Veljkovic:** Methodology, Supervision, Visualization, Writing – review & editing. **Henk Kolstein:** Data curation, Funding acquisition, Supervision, Writing – review & editing. **Johan Maljaars:** Data curation, Formal analysis, Supervision, Validation, Visualization, Writing – review & editing. **Richard Pijpers:** Data curation, Validation, Writing – review & editing.

Declaration of competing interest

The authors declare that they have no known competing financial interests or personal relationships that could have appeared to influence the work reported in this paper.

Data availability

Data will be made available on request.

Acknowledgements

This study is sponsored by the Dutch bridge asset owner Rijkswaterstaat (RWS). The authors acknowledge Frank van Dooren from RWS for his suggestions in the project meetings. The first author would like to thank China Scholarship Council for the study funding.

References

[1] Kolstein MH. Fatigue classification of welded joints in orthotropic steel bridge decks (doctoral thesis), Delft University of Technology; 2007.
[2] Maljaars J, Pijpers R, Wu W, Kolstein H. Fatigue resistance of rib to deck, crossbeam to deck and deck to deck welds in orthotropic decks using structural stress. Int J Fatigue 2023;175:107742.
[3] de Jong FBP. Renovation techniques for fatigue cracked orthotropic steel bridge decks (doctoral thesis), Delft University of Technology; 2007.
[4] Fu Z, Ji B, Zhang C, Wang Q. Fatigue performance of roof and U-rib weld of orthotropic steel bridge deck with different penetration rates. J Bridge Eng 2017;22(6):04017016.
[5] prTS 1993-1-901: Fatigue design of orthotropic bridge decks with the hot spot stress method (final draft). Brussels, Belgium: European Committe for Standardization; 2023.
[6] Fricke W. IIW guideline for the assessment of weld root fatigue. Weld World 2013;57(6):753–91.
[7] Wu W, Kolstein H, Veljkovic M. Fatigue resistance of rib-to-deck welded joint in OSDs, analyzed by fracture mechanics. J Constr Steel Res 2019;162.
[8] Connor R, Fisher J, Gatti W, Gopalaratnam V, Kozy B, Leshki B, McQuaid DL, Medlock R, Mertz D, Murphy T, Paterson D, Sorensen O, Yadlosky J. Manual for design, construction, and maintenance of orthotropic steel deck bridges. 2012, p. 262, (February). FHWA-IF-12-027.
[9] EN1993-1-9: Eurocode 3: Design of steel structures – Part 1-9: Fatigue. Brussels, Belgium: European Committe for Standardization; 2005.
[10] prEN 1993-1-9: Eurocode 3: design of steel structures – Part 1-9: Fatigue. doc n3751 (enquiry draft). Brussels, Belgium: European Committe for Standardization; 2023.
[11] JSSC: Fatigue design recommendations for steel structures. Tokyo, Japan: Japanese Society of Steel Construction; 2012.
[12] AASHTO: LRFD bridge design specifications. 6th ed.. Washington DC, United States: American Association of State Highway and Transportation Officials; 2012.
[13] Lazzarin P, Zambardi R. A finite-volume-energy based approach to predict the static and fatigue behavior of components with sharp V-shaped notches. Int J Fract 2001;112(3):275–98.
[14] Radaj D, Vormwald M. Advanced methods of fatigue assessment. Springer; 2013.
[15] Livieri P, Lazzarin P. Fatigue strength of steel and aluminium welded joints based on generalised stress intensity factors and local strain energy values. Int J Fract 2005;133:247–76.
[16] Lazzarin P, Livieri P. Notch stress intensity factors and fatigue strength of aluminium and steel welded joints. Int J Fatigue 2001;23(3):225–32.
[17] Zerbst U, Madia M, Vormwald M, Beier H. Fatigue strength and fracture mechanics – A general perspective. Eng Fract Mech 2018;198:2–23.
[18] Paris P, Erdogan F. A critical analysis of crack propagation laws. Trans ASME 1963;85(4):528–33.
[19] Nagy W. Fatigue assessment of orthotropic steel decks based on fracture mechanics (doctoral thesis), Ghent University; 2017.
[20] Heng J, Zheng K, Gou C, Zhang Y, Bao Y. Fatigue performance of rib-to-deck joints in orthotropic steel decks with thickened edge U-ribs. J Bridge Eng 2017;22(9):04017059.
[21] Dijkstra D, Nicolaas T. Vermoeiingsonderzoek reparatiemethode trog dekplaat verbindingen moerdijkbrug. TNO report 2000-CON-R4016, TNO Bouw, Rijswijk, The Netherlands (In Dutch); 2000.
[22] Wang P, Pei X, Dong P, Song S. Traction structural stress analysis of fatigue behaviors of rib-to-deck joints in orthotropic bridge deck. Int J Fatigue 2019;125:11–22.
[23] Yang H, Wang P, Qian H. Fatigue behavior of typical details of orthotropic steel bridges in multiaxial stress states using traction structural stress. Int J Fatigue 2020;141:105862.
[24] Yuan H. Optimization of Rib-to-Deck Welds for Steel Orthotropic Bridge Decks (master thesis), Virginia Polytechnic Institute and State University; 2011.
[25] Dung CV, Sasaki E, Tajima K, Suzuki T. Investigations on the effect of weld penetration on fatigue strength of rib-to-deck welded joints in orthotropic steel decks. Int J Steel Struct 2015;15(2):299–310.
[26] Fisher JW, Barsom JM. Evaluation of cracking in the rib-to-deck welds of the bronx–whitestone bridge. J Bridge Eng 2015;04015065.
[27] Maljaars J, Bonet E, Pijpers RJ. Fatigue resistance of the deck plate in steel orthotropic deck structures. Eng Fract Mech 2018;201:214–28.
[28] Ya S, Yamada K. Fatigue durability evaluation of trough to deck plate welded joint of orthotropic steel deck. Struct Eng / Earthq Eng 2008;25(2):33–46.
[29] Ya S. Fatigue durability evaluations of trough to deck plate welded details of orthotropic steel deck (doctoral thesis), Nagoya University; 2009.
[30] Bruls A. Measurement and interpretation of dynamic loads in bridges phase 3 fatigue behaviour of orthotropic steel decks - report eur 13378. Tech. rep., Commission of the European Communities; 1991.
[31] Hobbacher AF. In: Mayer C, editor. Recommendations for fatigue design of welded joints and components. IIW collection, 2nd edition. Cham: Springer International Publishing; 2016.
[32] BS 7608:2014+a1:2015: Guide to fatigue design and assessment of steel products. British standards, London: British Standards Institution; 2014.
[33] EN10025-2: Hot rolled products of structural steels. Part 2: technical delivery conditions for non-alloy structural steels. Brussels, Belgium: European Committe for Standardization; 2004.
[34] Kozy BM, Connor RJ, Paterson D, Mertz DR. Proposed revisions to AASHTO-LRFD bridge design specifications for orthotropic steel deck bridges. J Bridge Eng 2011;16(6):759–67.
[35] Tsakopoulos PA, Fisher JW. Fatigue resistance investigation for the orthotropic deck on the Bronx-Whitestone bridge. ATLSS report No. 02-05, 117 ATLSS Drive Bethlehem, PA, the United States; 2002.
[36] ISO 5817: Welding-fusion-welded joints in steel, nickel, titanium and their alloys (beam welding excluded)-quality levels for imperfections. 2014.
[37] Favi C, Campi F, Germani M, Mandolini M. A data framework for environmental assessment of metal arc welding processes and welded structures during the design phase. Int J Adv Manuf Technol 2019;105(1–4).
[38] Konda N, Nishio M, Ichimiya M, Kasugai T, Kiyokawa S. Development of fatigue test method and improvement of fatigue life by new functional steel plates for welding of trough rib and deck plate of orthotropic decks. Int J Steel Struct 2013;13:191–7.
[39] Wu W, Kolstein H, Veljkovic M, Pijpers R, Vorstenbosch-krabbe J. Fatigue behaviour of the closed rib to deck and crossbeam joint in a newly designed orthotropic bridge deck. ce/papers 2017;1(2–3):2378–87.
[40] EN 1990: Eurocode—basis of structural design. Brussels, Belgium: European Committe for Standardization; 2002.
[41] Bartsch H, Drebenstedt K, Seyfried B, Feldmann M, Kuhlmann U, Ummenhofer T. Analysis of fatigue test data to reassess EN 1993-1-9 detail categories. Steel Constr 2020;13(4):280–93.
[42] Simulia. Abaqus user's manual version 2019. 2019.
[43] Bäckström M, Marquis G. A review of multiaxial fatigue of weldments: Experimental results, design code and critical plane approaches. Fatigue Fract Eng Mater Struct 2001;24(5):279–91.
[44] Park W, Miki C. Fatigue assessment of large-size welded joints based on the effective notch stress approach. Int J Fatigue 2008;30(9):1556–68.
[45] Pedersen MM. Multiaxial fatigue assessment of welded joints using the notch stress approach. Int J Fatigue 2016;83:269–79.
[46] Lazzarin P, Berto F, Zappalorto M. Rapid calculations of notch stress intensity factors based on averaged strain energy density from coarse meshes: Theoretical bases and applications. Int J Fatigue 2010;32(10):1559–67.
[47] Chapetti MD, Steimbreger C. A simple fracture mechanics estimation of the fatigue endurance of welded joints. Int J Fatigue 2019;125:23–34.
[48] Fischer C, Feltz O, Fricke W, Lazzarin P. Application of the notch stress intensity and crack propagation approaches to weld toe and root fatigue. Weld World 2011;55(7):30–9.